Fibers and Polymers (2024) 26:1197–1208
https://doi.org/10.1007/s12221-024-00825-9

Online ISSN 1875-0052
Print ISSN 1229-9197

REGULAR ARTICLE

Magnetic Biochar Production from Agricultural Waste and Reactive Blue 19 Removal by Peroxymonosulfate Activation

Neslihan Kader[1] · Gökçe Didar Değermenci[1]

Received: 26 February 2024 / Revised: 21 August 2024 / Accepted: 15 December 2024 / Published online: 31 December 2024

Abstract
The conversion of agricultural biomass waste into value-added biochar (BC)-based catalysts is of great interest. Magnetic biochar is an excellent material that facilitates both solid–liquid separation and peroxymonosulfate (PMS) activation. In this study, magnetic biochar was produced from pea pod, an agricultural waste, by pyrolysis, hydrothermal methods, and precipitation. The structure, morphology, and magnetic separation properties of magnetic biochar produced from pea pod (MPPBC) were comprehensively analyzed by different characterization methods. Reactive blue 19 (RB19) was selected as a model pollutant to evaluate the performance of the MPPBC/PMS system. The effect of initial solution pH, MPPBC dosage, PMS concentration, initial RB19 concentration, reusability, and concentrations of anions and natural organic matter concentrations on the removal of RB19 in the MPPBC/PMS system was investigated. The results showed that MPPBC could effectively activate PMS, and RB19 removal reached 85% at an initial solution pH of 3, an MPPBC dosage of 0.20 g/L, a PMS concentration of 0.50 mM, an initial RB19 concentration of 25 mg/L, and an oxidation time of 60 min. The reusability of MPPBC showed an 8% decrease in the removal efficiency of RB19 after four uses. Anions and natural organic matter added to the solution were found to decrease the removal of RB19. The kinetics of RB19 removal in MPPBC/PMS system was determined using first order, second order, and Behnajady-Modirshahla-Ghanbery (BMG) models. As a result of kinetic calculations, the BMG kinetic model was found to be more effective for describing the removal efficiency of RB19.

Keywords Pea pod · Magnetite biochar · Peroxymonosulfate activation · Reactive blue 19 · Advanced oxidation process

1 Introduction

The textile, printing and dyeing, paper, food, and leather industries have developed with the rapid urbanization and industrialization in recent years. As these industries grow, water consumption for producing and applying dyes is increasing [1]. A considerable amount of paint wastewater is produced globally, with over 700,000 tons of paint produced annually, and 5–10% of these dyes are mixed with industrial wastewater [2]. Chemically persistent and non-biodegradable dyes pose a serious threat to living organisms and the environment [3]. The discharge of dye-containing water into receiving waters can cause health problems (e.g., carcinogenicity and toxicity) for living organisms by blocking the passage of sunlight, slowing the rate of photosynthesis and leading to a decrease in dissolved oxygen [4]. The molecular structures of strongly colored reactive dyes contain a chromophore group (azo, anthraquinone, phthalocyanine, and triarylmethane) and a functional group that can form covalent bonds with cellulose fibers [5]. Reactive blue 19 (RB19) is an anthraquinone-based vinyl sulfone dye that has gained popularity due to its strong dyeing properties, high color value and remarkable dispersibility. With a half-life of 46 years, the RB19 molecule has exceptionally stable chemical properties due to its encapsulation with an anthraquinone ring [1]. Wastewater containing RB19 that is released into a receiving environment untreated or insufficiently treated poses a risk to human health as well as the ecosystem. The main amine groups in RB19's chemical structure have the ability to interact with DNA, changing the genetic material in the process. Long-term carcinogenic effects can result from such genetic alterations that impair cells' normal ability to function [2]. Treatment processes developed to reduce the environmental impact of wastewater

✉ Gökçe Didar Değermenci
gdegermenci@kastamonu.edu.tr

[1] Department of Environmental Engineering, Kastamonu University, 37150 Kastamonu, Türkiye

containing reactive dyes are of great importance. Adsorption and advanced oxidation processes are among the most effective methods for the treatment of reactive dyes, and extensive research has been carried out in this field Intensified degradation of reactive blue [6, 7]. However, adsorption can only transfer dye molecules from the liquid phase to the solid phase, which leads to secondary pollution problems. Furthermore, regenerating spent adsorbents requires costly recycling steps [8]. The most commonly used adsorbent worldwide in recent years is activated carbon/biochar, which has highly developed pore properties and functional surface groups. Biochar is a material that can be obtained by pyrolysis from biomass, a particularly sustainable resource. One advantage of biomass is its low carbon footprint. Carbon materials obtained from biomass can be easily modified by doping with various metal oxide [9].

Advanced oxidation processes (AOPs) conducted by metal oxides are widely used in the degradation of organic substances [10]. In these processes, the types of radicals generated or utilized determine the oxidation capacity. Sulfate radical systems have a longer half-life, a broader pH range of application, and a stronger oxidation ability than hydroxyl radical systems. Peroxymonosulfate (PMS) and peroxydisulfate (PDS) are the main sources of sulfate radicals ($SO_4^{\cdot-}$). PMS has an asymmetric molecular structure and a stronger activation performance. Therefore, PMS is more common and popular in practical applications. PMS has an asymmetric molecular structure and oxidizing properties, which can generate reactive oxygen species (ROS) such as free radicals through the activation of electricity, heat, microwave, ultraviolet light, alkali, ultrasound, and transition metals [1, 11]. Iron-based catalysts (e.g., Fe^{2+}, FeCN, Fe_2O_3, Fe_3O_4) are widely preferred in various water treatment processes for the degradation of resistant organic pollutants. These catalysts are preferred for their cost-effectiveness and environmentally friendly properties [12]. Magnetite (Fe_3O_4) can be easily separated from wastewater by magnetic separation, which makes the separation and recycling of the catalyst simple and cost-effective [13]. However, these iron oxide nanoparticles have a problem of agglomeration due to their high gravitational force. In order to prevent this, synthetic materials are created by coating nanoparticles on biochar [14]. Effective solutions are presented in the literature for the removal of dyes using biochar with magnetic properties based on sulfate radical production. For example, Fe/Mn biochar composite produced from sugarcane waste was used for PMS activation to catalyze azo dye removal by oxidation [15]. Another study investigated the performance of nZVI/MoS_2-BC as an activator for PMS to remove dyes, antibiotics and endocrine disruptors in water [16]. In another study, research was carried out on methylene blue removal by persulfate activation using magnetic biochar obtained with collagen fiber and iron addition [17].

The use of biochar and nanocomposites synthesized from pea pod as low-cost and environmentally friendly catalysts based on the reuse of agro-industrial waste can offer a sustainable solution for the treatment of water contaminated with dyes. The aim of this study is to produce biochar from pea pod, an agricultural waste, and then to obtain magnetic biochar by hydrothermal and precipitation method with the addition of iron. When the produced magnetic biochar is used for PMS activation, it can enhance the oxidative degradation of organic pollutants, providing high efficiency in water treatment. Additionally, its magnetic properties allow it to be easily separated and reused. In the literature, no studies have been found on the removal of RB19 through PMS activation using magnetic biochar. This gap highlights the need to explore the potential of magnetic biochar as an effective solution for the removal of harmful dyes like RB19. Therefore, in this study, the produced magnetic biochar was used for PMS activation, and its effectiveness in removing RB19 was investigated. In this context, the effects of initial pH, initial PMS concentration, catalyst amount, initial RB19 concentration, inorganic anions, natural organic matter and catalyst reusability were investigated and kinetic studies were carried out.

Table 1 RB19 properties and chemical structure

Parameters	Values
Generic name	Reactive Blue 19
Commercial name	Remazol Brilliant Blue R
Abbreviation	RB19
Functional group	Anthraquinone
Molecular weight (g/mol)	626.54
λ_{max} (nm)	593
Chemical formula	$C_{22}H_{16}O_{11}N_2S_3Na_2$
Molecular formula	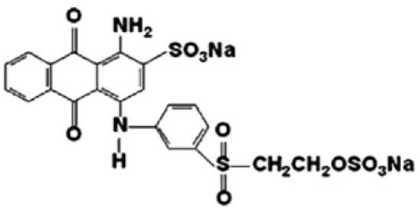

2 Materials and Methods

2.1 Chemical Substances and Reagents

The dye RB19 was obtained from a textile factory in Bursa, Turkey. RB19 was selected because it is widely used in the textile industry, especially in the dyeing of cotton, silk, nylon, and wool. The properties and molecular structure of RB19 are listed in Table 1. All chemicals and reagents used in the study were of analytical purity. The sources for these chemicals were as follows: potassium peroxymonosulfate (Oxone) and $FeSO_4{\cdot}7H_2O$ were obtained from Acros Organics; ethanol and sodium carbonate were obtained from Carlo Erba; $FeCl_3{\cdot}6H_2O$ and NaOH were obtained from Merck and H_2SO_4 and HCl were obtained from Sigma. The stock solution of RB19 dye was prepared by dissolving 1000 mg of dye in 1 L of distilled water, and subsequent working concentrations were obtained by successive dilutions of the stock solution. The initial pH of each run was adjusted with 0.1 M NaOH and H_2SO_4 solutions before mixing.

2.2 Magnetic Biochar Preparation

The pea pods (PP) used in this study were obtained as a waste product from local producers in Kastamonu, Turkey. The samples were dried in an oven at 60 °C for 3 days. The dried samples were crushed and sieved to obtain a particle size between 250 and 500 µm. The pea pods were then stirred in a 20% Na_2CO_3 solution for 30 min, kept in this solution overnight, and dried to constant weight. The dried pea pods were carbonized in a muffle furnace at 500 °C for 2 h at a heating rate of 27 °C/min in a nitrogen gas environment. After the carbonized sample reached room temperature, it was kept in 0.1 M HCl until no gas bubbles formed. It was then washed with distilled water to a neutral pH and dried at 105 °C. This sample was called pea pod biochar (PPBC). A series of treatments were carried out to impart magnetic properties to the PPBC. 3 g of $FeCl_3{\cdot}6H_2O$ and 3 g of $FeSO_4{\cdot}7H_2O$ were added to a solution containing 100 mL of distilled water and 50 mL of ethanol. After adding 1 g PPBC to the iron-containing synthetic solution, it was heated in a hydrothermal reactor for 12 h in an oven at 180 °C with a heating rate of 4 °C/min and cooled to room temperature. The pH was then raised to alkalinity by adding 1 M NaOH dropwise until a black precipitate formed and precipitation was carried out. The resulting black precipitate was washed with ethanol and then washed several times with distilled water. Finally, it was dried overnight in an oven at 105 °C and named magnetic pea pod biochar (MPPBC).

2.3 Experimental Procedure

Oxidation experiments were carried out in a glass reactor containing RB19 in a solution volume of 100 mL. The temperature and stirring speed of the solution containing dye were 25 ± 1 °C and 500 rpm, respectively. First of all, the initial pH value of the solution was adjusted, then PMS was added and stirred for 2 min and then MPPBC was added and oxidation experiments were started. Samples taken at certain time intervals were centrifuged at 3000 rpm for 2 min and then analyzed for RB19. RB19 concentration was measured using a UV–vis spectrophotometer (Hach Lange DR6000) at maximum wavelength ($\lambda = 593$ nm). The removal efficiency of RB19 was calculated according to Eq. (1):

$$\text{Percentage removal}(\%) = \left(1 - C/C_0\right) \times 100 \tag{1}$$

Then, the effect of various experimental parameters on RB19 removal such as initial solution pH (3–9), MPPBC dosage (0.05–0.40 g/L), PMS concentration (0.10–1.00 mM), initial RB19 concentration (25–75 mg/L), and the effect of some ions that may be present in the water bodies were investigated.

2.4 Kinetic Analysis

RB19 dye removal was modeled using first-order (Eq. (2)), second-order (Eq. (3)), and Behnajady-Modirshahla-Ghanbery (BMG) (Eq. (4)) kinetic models [18]. The coefficients of the models used were calculated using the nonlinear method with the help of Microsoft Excel Solver add-in.

$$C = C_0 \times e^{-k_1 \times t} \tag{2}$$

$$C = C_0 / \left(1 + C_0 \times k_2 \times t\right) \tag{3}$$

$$C = C_0 \times \left[1 - t/(m + b \times t)\right] \tag{4}$$

where C_0 and C (mg/L) are the initial RB19 concentration and the RB19 concentration at any time t respectively; k_1 (min^{-1}) and k_2 (L/mg/min) are the first and second order rate constants, respectively; b and m (min) represent the theoretical oxidation and reaction kinetics for the BMG model, respectively. b and m parameters represent the initial degradation rate ($1/m$) and the maximum theoretical degradation fraction ($1/b$) of pollutants in the process.

2.5 Characterization of Catalyst

A scanning electron microscope (SEM, FEI Quanta FEG 250) operated at 15 kV was used to study the morphological properties of MPPBC, while an X-ray diffractometer (XRD, Bruker D8 Advance) was used to study its crystallographic

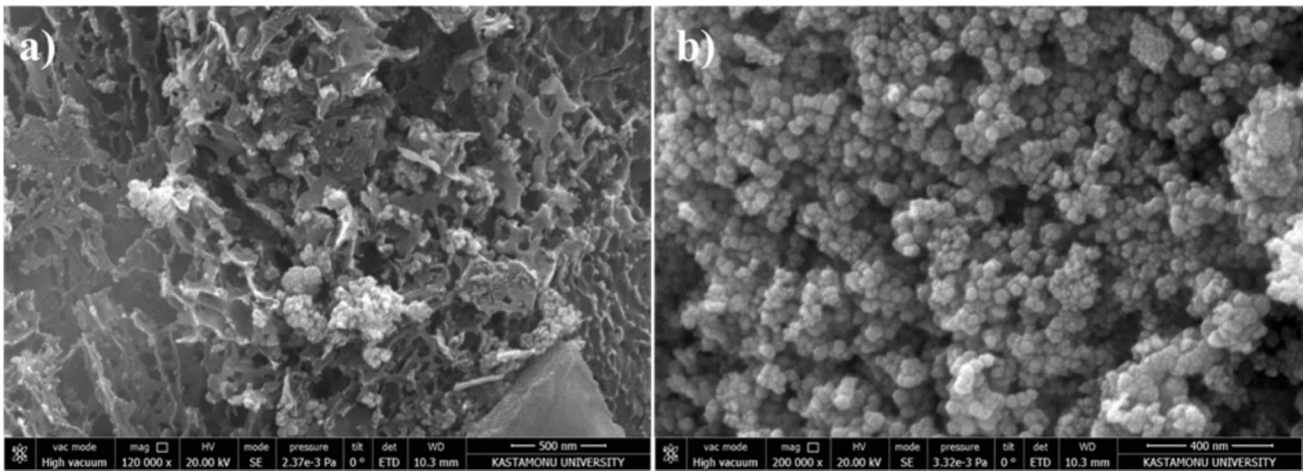

Fig. 1 SEM images of MPPBC

properties. An Attenuated Total Reflectance Fourier Transform Infrared (ATR-FTIR, Bruker Alpha II) in the spectral range 400–4000 cm^{-1} (resolution 4 cm^{-1}, scans 24) was used to determine the functional groups. Specific surface area was estimated by Brunauer–Emmett–Teller (BET, Quantachrome Nova Touch LX4), while pore volume and size were measured using the Barrett-Joyner-Halenda (BJH) formula. The magnetic properties of MPPBC were measured at room temperature with a Vibrating Sample Magnetometer (VSM, Lake shore 7407).

3 Results and Discussion

3.1 Characterization of MPPBC

The morphological structure and the distribution of the surface elements of MPPBC are shown in Fig. 1. Figure 1a shows that MPPBC has a porous structure and a rough surface. It can be seen that the surface of the biochar is successfully coated with iron oxide nanoparticles. However, at higher magnification (Fig. 1b), it can be seen that the iron oxide nanoparticles have a regular spherical morphology and a particle size in the range of about 28–46 nm. BET surface area analysis shows that the surface area of the prepared MPPBC is 64.62 m^2/g, the average pore diameter is 8.532 nm, and the pore volume determined by the Barrett-Joyner-Halenda (BJH) method is 0.259 cm^3/g.

The crystal structure and composition of the synthesized MPPBC were determined by XRD (Fig. 2). The powder XRD pattern of MPPBC showed the presence of iron oxides such as maghemite (JCPDS card number 00-039-1346) and magnetite (JCPDS card number 01-076-1849). Six diffraction peaks with the following positions and Miller indices were identified in the XRD pattern of MPPBC: 30.3° (220),

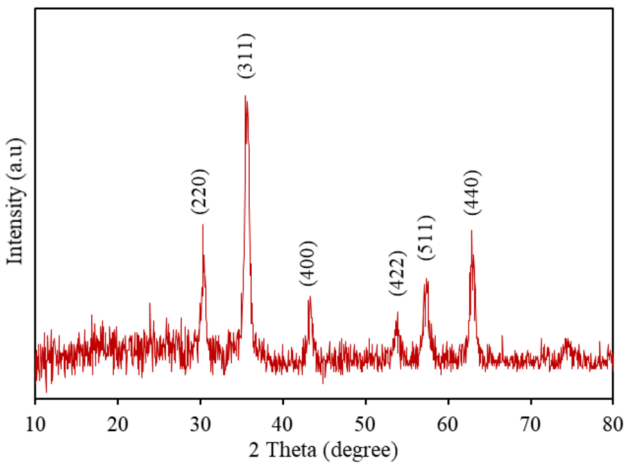

Fig. 2 XRD patterns of synthesized MPPBC

35.46° (311), 43.30° (400), 53.70° (422), 57.12° (511), and 62.90° (440) [19]. The most intense line is the one located at 35.46°. Maghemite and magnetite phases are very difficult to identify by X-ray diffraction because both phases have the same spinel structure and almost identical lattice parameters [20].

Functional groups on the surface of PPBC and MPPBC were investigated using FTIR spectroscopy (Fig. 3). The region between 4000 and 1450 cm^{-1} contains various functional groups, while the region between 1450 and 500 cm^{-1} is called the fingerprint region [21]. In the FTIR spectrum, the peak at 3349 cm^{-1} indicates the presence of OH stretching vibration. This indicates interlayer crystalline water or hydroxyl groups in PPBC/MPPBC [22, 23]. The peak at 1581 cm^{-1} was attributed to aromatic C=C stretching [24] and the peaks at 1233 cm^{-1} and 1133 cm^{-1} to C–O stretching vibrations [25]. The new peaks at 555 and 632 cm^{-1} on

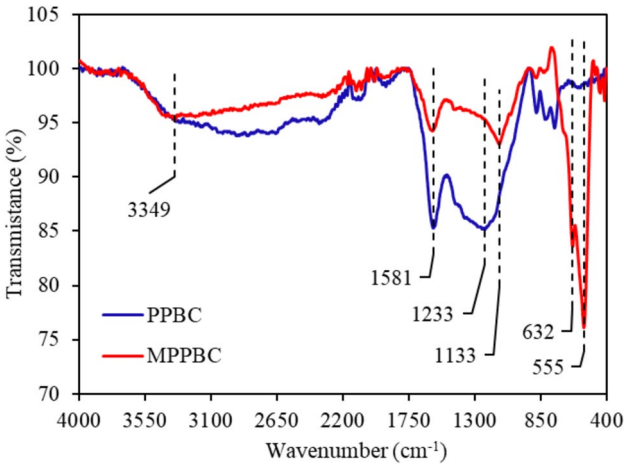

Fig. 3 FTIR spectra of PPBC and MPPBC samples

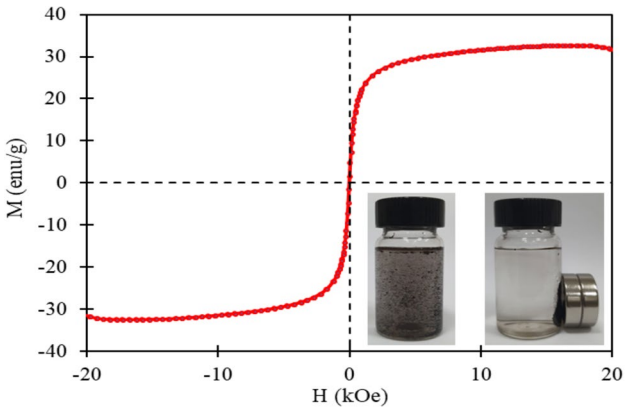

Fig. 4 VSM result of magnetic biochar and its attraction with magnet in aqueous media

the MPPBC surface are attributed to adsorption peaks associated with the Fe–O stretching vibration [26, 27], indicating the formation of Fe oxides on the MPPBC surface.

The VSM technique was used to investigate the magnetic behavior of MPPBC. A magnetic field of ± 20 kOe was applied to the MPPBC sample and the obtained magnetization values were measured at room temperature. The hysteresis curve obtained with the VSM device is shown in Fig. 4. It can be said that MPBBC exhibits superparamagnetic properties with a saturation magnetization value of about 32.63 emu/g [28]. As shown in Fig. 4, MPPBC can be easily separated magnetically from aqueous solution. In a study reported that despite the low saturation magnetization value (12.32 emu/g) of the material containing clay/Fe_3O_4 composite particles, it can be separated from aqueous solution by applying a simple external magnetic field [29].

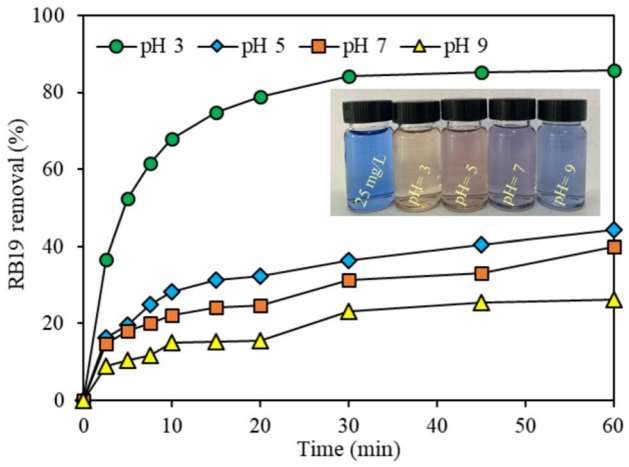

Fig. 5 Effect of different initial solution pH value on RB19 removal in MPPBC/PMS system (MPPBC = 0.2 g/L, PMS = 0.5 mM, RB19 = 25 mg/L)

3.2 Influence of Initial Solution pH

The pH value of the initial solution is one of the important factors for peroxymonosulfate (PMS) activation, due to its strong influence on the decomposition of PMS to form reactive oxygen species (ROS) [30]. Below a solution pH of 7, sulfate radicals are the predominant reactive species [31]; however, at neutral pH, hydroxyl and sulfate radicals are equally involved in the reactions. Similarly, peroxymonosulfate (HSO_5^-) can be activated to form sulfate radicals [32]. Therefore, the effect of the initial solution pH on the removal of RB19 in the MPPBC/PMS system was investigated. To determine the effect of initial solution pH on RB19 removal, experiments were performed with different initial solution pH values at an initial RB19 concentration of 25 mg/L, an MPPBC dosage of 0.2 g/L and a PMS concentration of 0.5 mM. Figure 5 shows the effect of initial solution pH (3, 5, 7, and 9) on RB19 removal. When the initial pH of the solution was 3, 5, 7, and 9, the RB19 removal efficiency was 85.8%, 44.4%, 40.1%, and 26.2%, respectively, at a reaction time of 60 min. It was observed that the removal efficiency of RB19 decreased with increasing pH of the initial solution, suggesting that the activation ability of PMS decreases with increasing pH of the initial solution. This indicates that acidic conditions are beneficial for the catalytic reaction, which is consistent with previous studies [33]. Under acidic conditions, electrostatic attraction promotes the adsorption of PMS by the catalyst, which facilitates the transport of electrons and the activation of PMS to form sulfate radicals (Eq. (5)) [34]. In addition, the initial pH of the solution can also influence the structural form of iron species and target contaminants [35, 36]. An increase in the pH value of the solution can favor the conversion of sulfate radicals into

hydroxyl radicals (Eq. (6)) [37]. Compared to the hydroxyl radical, the sulfate radical has a higher oxidation potential (2.5–3.1 V) [34], so it can provide a higher reaction rate for the removal of RB19. However, under alkaline conditions, the dissolution of Fe^{2+} on the surface of iron oxide nanoparticles can be inhibited and passivate the surface of these nanoparticles [38, 39]. As a result, the amount of sulfate radical formed and consequently the removal efficiency of RB19 decreases with increasing pH of the solution.

$$HSO_5^- + Fe^{2+} \rightarrow SO_4^{\bullet -} + Fe^{3+} + OH^- \quad (5)$$

$$SO_4^{\bullet -} + OH^- \rightarrow SO_4^{2-} + OH\cdot \quad (6)$$

3.3 Influence of Catalyst Dosage

Catalyst dosage in PMS activation has a significant impact on the removal of target pollutants [40, 41]. Therefore, the effect of catalyst dosage on the removal of RB19 in the MPPBC/PMS system was investigated and the results are shown in Fig. 6. To determine the effect of catalyst dosage on RB19 removal, experiments were conducted with different catalyst dosages at an initial RB19 concentration of 25 mg/L, an initial solution pH of 3, and a PMS concentration of 0.5 mM. Figure 6a shows the effects of different catalyst dosages (0.05–0.4 g/L) on RB19 removal. The results show that RB19 dye is significantly dependent on the MPPBC dosage. At the end of the 60 min reaction time, RB19 removal is 80.0%, 83.6%, 85.8% and 86.6% at catalyst dosages of 0.05, 0.1, 0.2 and 0.4 g/L (MPPBC), respectively. At a reaction time of 30 min, the RB19 removal with increasing catalyst dosage was 60.4%, 71.6%, 84.2% and 82.9%, respectively. Increasing the catalyst dosage led to an increase in the surface area and thus to an increase in the RB19 removal rate. For reaction times higher than 30 min, no significant improvement in RB19 removal efficiency was observed when the catalyst dosage was increased from 0.20 to 0.40 g/L. A higher catalyst dosage than 0.40 g/L was not tested due to the scavenging effect on the radicals formed [36]. In a study, it was observed that increasing the catalyst dosage from 0.2 to 1.0 g/L led to an increase in degradation efficiency from 74.41 to 90.41% after 60 min for the removal of tetracycline hydrochloride. These results suggest that higher catalyst dosages positively influence the degradation rate of tetracycline hydrochloride [42]. Consequently, faster removal of RB19 can be achieved by optimizing the contact time and catalyst dosage in the MPPBC/PMS system. Similar results were observed for the removal of bisphenol A, moxifloxacin and *p*-chlorophenol [43–45]. Considering the cost and RB19 removal, the optimum catalyst dosage

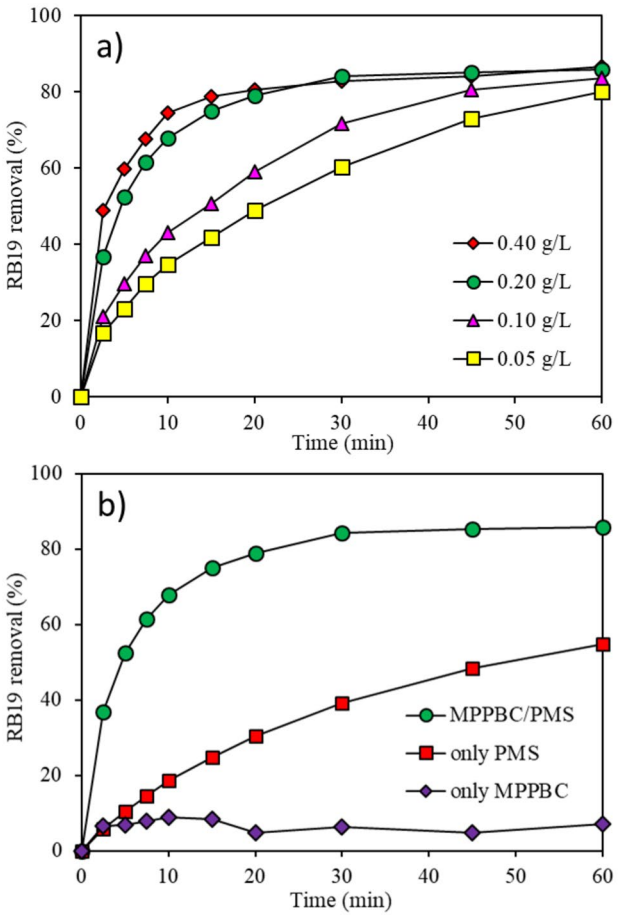

Fig. 6 Effect of MPPBC dosage (**a**) and different reaction systems (**b**) on RB19 removal in MPPBC/PMS system (initial pH = 3, PMS = 0.50 mM, RB19 = 25 mg/L)

for the MPPBC/PMS system was 0.20 g/L. The removal of RB19 in the MPPBC/PMS system was studied only in the presence of MPPBC and only in the presence of PMS (MPPBC = 0.2 g/L, PMS = 0.5 mM, RB19 = 25 mg/L, initial pH = 3). The results obtained are shown in Fig. 6b. When only PMS was used, RB19 removal was 54.7% in 60 min reaction time. Then the removal of RB19 by adsorption was investigated in the experiment where only MPPBC was used. At the end of 60 min, RB19 removal by adsorption was found to be 7.0%. When MPPBC and PMS were used together, RB19 removal increased to 85.8%. The combined use of MPPBC and PMS had a synergistic effect and increased RB19 removal by 24.1%. This effect can be attributed to the activation of PMS by MPPBC.

3.4 Influence of PMS Concentration

In addition to the catalyst dosage, the PMS concentration is another equally important factor in the oxidation reaction [46]. To determine the effect of PMS concentration in

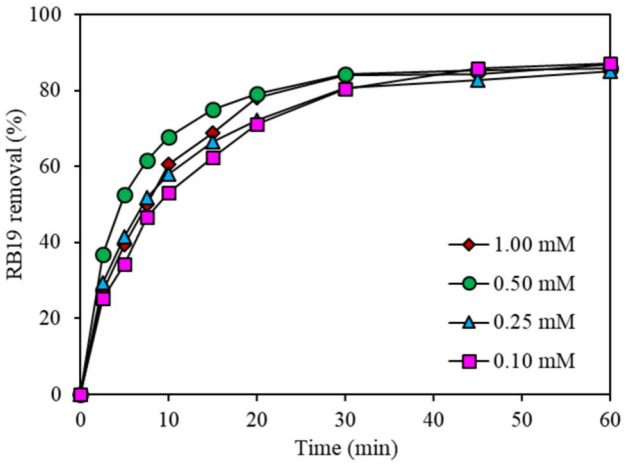

Fig. 7 Effect of PMS dosage on RB19 removal in MPPBC/PMS system (initial pH = 3, MPPBC = 0.2 g/L, RB19 = 25 mg/L)

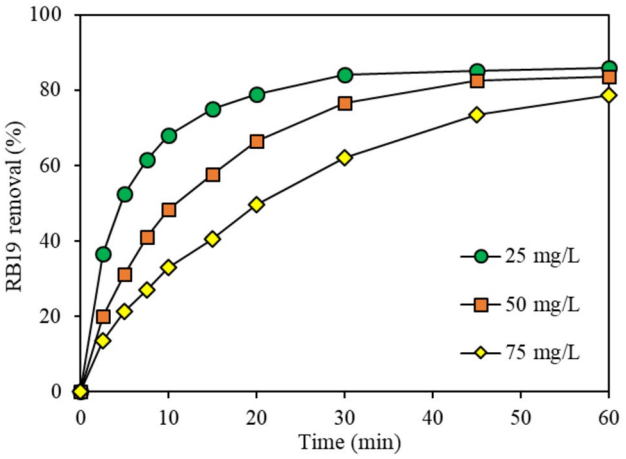

Fig. 8 Effect of initial RB19 concentration on removal efficiency in MPPBC/PMS system (initial pH = 3, MPPBC = 0.2 g/L, PMS = 0.5 mM)

the MPPBC/PMS system, RB19 dye removal experiments were performed at 4 different PMS concentrations (0.10, 0.25, 0.50, and 1.00 mM) with an initial RB19 concentration of 25 mg/L, an MPPBC dosage of 0.2 g/L and an initial solution pH of 3. The results are shown in Fig. 7. For different PMS concentrations, the RB19 removal ranged from 85.1% to 87.0% with a reaction time of 60 min. Therefore, it can be said that PMS concentration has no significant effect on RB19 removal efficiency for 60 min reaction time in MPPBC/PMS system. The removal rate of RB19 was found to increase with increasing PMS concentration from 0.10 mM to 0.50 mM. The highest removal rate was obtained at 0.50 mM. The removal rate of RB19 decreased with increasing PMS concentration to 1.00 mM. This is due to the fact that excessive addition of PMS prevented the effective utilization of sulfate radicals and hydroxyl radicals (Eqs. (7) and (8)) [45, 47]. However, it can also be the production of peroxydisulfate without oxidation performance by the self-quenching effect of sulfate radicals according to the reaction given in Eq. (9) [48]. A study using Fe/Mn-biochar composite evaluated the effect of PMS concentration on the degradation efficiency of Orange G. It was reported that for 0.1 g/L Orange G, increasing PMS dosage from 0 to 1.0 mM enhanced the degradation efficiency from 5 to 96%, but further increasing PMS dosage from 1.0 mM to 1.5 mM did not increase this efficiency [15].

$$SO_4^{\cdot-} + HSO_5^- \rightarrow SO_5^{\cdot-} + HSO_4^- \quad (7)$$

$$OH\cdot + HSO_5^- \rightarrow SO_5^{\cdot-} + H_2O \quad (8)$$

$$SO_4^{\cdot-} + SO_4^{\cdot-} \rightarrow S_2O_8^{2-} \quad (9)$$

3.5 Influence of RB19 Concentration

To determine the effect of initial RB19 concentration on removal efficiency in the MPPBC/PMS system, experiments were performed with three different RB19 concentrations (25, 50, and 75 mg/L) at an initial solution pH of 3, an MPPBC dosage of 0.2 g/L and a PMS concentration of 0.50 mM. The results obtained are shown in Fig. 8. At concentrations above 25 mg/L, the RB19 removal efficiency decreased. For initial RB19 concentrations of 25, 50, and 75 mg/L, the RB19 removal efficiency at 60 min reaction time is 85.8%, 83.4%, and 78.7%, respectively. At a reaction time of 30 min, the RB19 removal efficiency with increasing initial RB19 concentration is 84.2%, 76.6%, and 62.1%, respectively. The decrease in removal efficiency with increasing RB19 concentration may be attributed to the fact that the amount of radicals generated during the reaction is insufficient for the removal of high RB19 concentrations. As the RB19 concentration increases, the amount of organic matter in the sample increases. As a result, the competitive consumption of radicals increases. On the other hand, during the degradation of these organic substances, intermediates are formed that can consume the radicals generated in the MPPBC/PMS system. As a result, the ratio of radicals to RB19 decreases, which reduces the RB19 removal efficiency [49]. Since the concentrations of the catalyst and oxidant are the same in the MPPBC/PMS system are the same, the concentrations of radicals formed in solution are also the same. Therefore, a longer removal time is required for a higher concentration of RB19 in solution [50]. The RB19 removal rates showed an increasing trend with decreasing initial RB19 concentration. It can be said that at low RB19

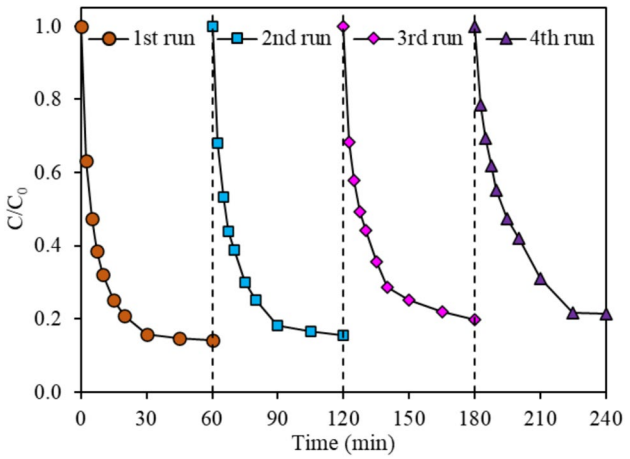

Fig. 9 Reusability experiments of MPPBC (initial pH = 3, MPPBC = 0.2 g/L, PMS = 0.5 mM, RB19 = 25 mg/L)

concentration, the system is able to produce a sufficient amount of ROS, some of which can fully interact with RB19 molecules. However, at lower pollutant concentrations, some of the useless ROS may be wasted, leading to a mismatch and wasteful phenomenon in the degradation load of the system [2].

3.6 Stability Studies of MPPBC

The stability and recyclability of catalysts are critical factors for practical applications. Most catalysts produced from biochar are difficult to recycle because they are in powder form. To increase the recyclability of biochar, it can be magnetized so that it can be very easily separated from the solution, which not only significantly increases recyclability but also prevents secondary pollution of the water. However, most of the carbonized catalysts for PMS activation presented so far have low stability and the catalytic performance degrades rapidly when reused [51]. Four experimental cycles were carried out to evaluate the stability of MPPBC (Fig. 9). As can be seen from the Fig. 9, the removal efficiency of RB19 decreased slightly after each use. The removal efficiency of RB19 decreased from 87 to 84%, 80%, 80%, and 79% in four cycles. The removal efficiency of RB19 when MPPBC was reused decreased by 8% after the fourth cycle. There may be two reasons for this slight decrease. One is that the deactivation of some active sites leads to a decrease in catalytic performance. The other reason could be that the RB19 adsorbed on the catalyst was oxidized by ROS and converted into intermediates, which were also adsorbed on the catalyst [16]. Previous studies have shown similar trends in catalyst reusability. For instance, a study investigating tetracycline removal via PMS activation using magnetic biochar reported a decrease in tetracycline removal efficiency from 79.89% during the first use to 54.91% by the fourth use [52]. In another study, $MnFe_2O_4$ magnetic biochar was found to exhibit a reduction in orange II removal efficiency from 100% in the first cycle to 50% and 46% in the second and third cycles, respectively [53]. Additionally, research on the reusability of the magnetic Fe_3S_4/biochar composite observed a decreasing trend in degradation efficiency with increased cycle number, although 2,4,6-trichlorophenol achieved a degradation efficiency of 61.7% after five cycles [54]. In this context, MPPBC demonstrated superior stability and recycling potential compared to other catalysts. Particularly, the efficiency of MPPBC showed only an 8% decrease over four cycles, indicating its ability to maintain performance even during extended use.

3.7 Influence of HA and Anions

Inorganic anions (Cl^-, NO_3^-, PO_4^{3-}, CO_3^{2-}, HCO_3^-, and others) and natural organic matter (NOM) are frequently detected in water bodies. Reactive species generated in AOPs (hydroxyl radicals, sulfate radicals, superoxide radicals, and hydroperoxyl radicals) can react with inorganic anions and NOM present in the water matrix, leading to the conversion of reactive species and having positive/negative effects on the performance of AOPs [2, 55]. Therefore, it is very important to investigate the effects of inorganic anions and NOM on the oxidation system [56]. Therefore, the potential effects of chloride (Cl^-), dihydrogen phosphate ($H_2PO_4^-$), nitrate (NO_3^-) and humic acid (HA) on the removal of RB19 in the MPPBC/PMS system were investigated. The results obtained are shown in Fig. 10. It was found that RB19 removal decreased with the addition of HA and other anions.

In Fig. 10, the RB19 removal is 85.8% at 60 min oxidation time in the absence of HA and other anions. When Fig. 10a is examined, it is seen that RB19 removal decreases with the addition of HA to the solution medium. At an oxidation time of 60 min, RB19 removal of 80.1% was obtained at an HA concentration of 1 mg/L, while RB19 removal decreased to 68.9% when the HA concentration was increased to 5 mg/L. This effect can be attributed to two reasons: i) HA may react with ROS to decrease RB19 removal [35]; ii) HA tends to close the active sites by adsorption on the catalyst surface, which may decrease the activation of PMS with MPPBC and reduce RB19 removal efficiency [57]. Similarly, in a study, for RB19 removal, increasing the HA concentration from 0 mg/L to 20 mg/L causes the removal efficiency to decrease from 100 to 21%. They stated that this negative effect is related to the capacity of HA to consume radical species and its ability to coat the active surfaces of the catalyst [58].

Figure 10b shows that the added Cl^- prevents the removal efficiency of RB19. RB19 removal decreased from 81.2 to 78.3% when the Cl^- concentration increased from 1 to 5 mM. This decrease may be due to the formation of

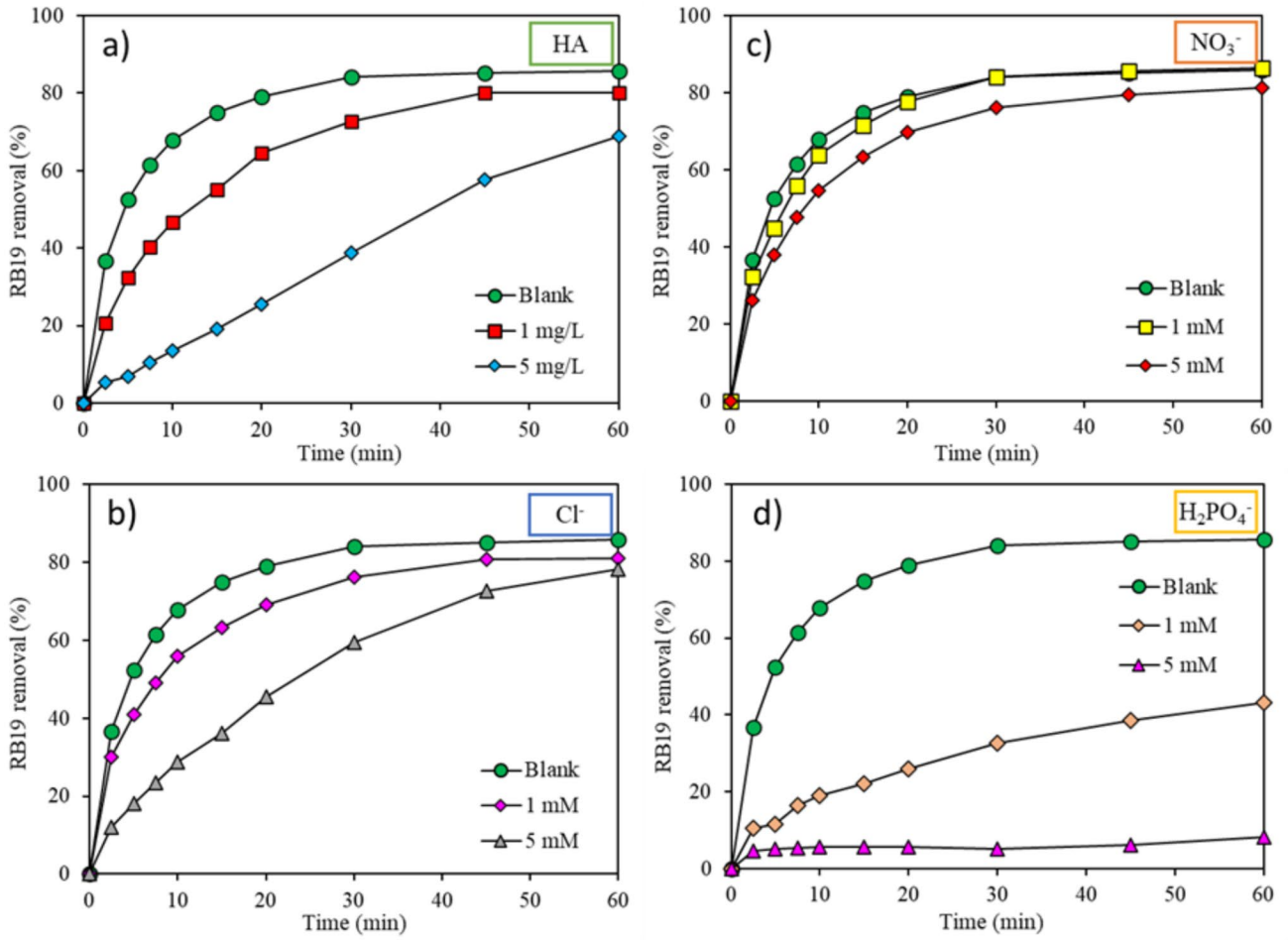

Fig. 10 Effects of HA (**a**), Cl^- (**b**), NO_3^- (**c**), and $H_2PO_4^-$ (**d**) on the removal of RB19 by MPPBC/PMS system (initial pH = 3, MPPBC = 0.2 g/L, PMS = 0.5 mM, RB19 = 25 mg/L)

secondary chlorine radicals with lower redox potential as a result of the reactions between Cl^- and $SO_4^{\cdot-}$ and OH radicals (Eqs. (10)-(13)) [35, 43, 47, 51]. The chlorine radicals $Cl^{\cdot}$ and $Cl_2^{\cdot-}$ have a lower reduction potential than hydroxyl radicals [55, 59, 60]. In addition, Cl^- can react with PMS and form reactive halogens (Eqs. (14) and (15)) (HOCl and Cl_2), which impair the degradation of organic pollutants [43]. Thus, chloride ions may affect the stability of PMS and reduce the removal of RB19. These reasons may have inhibited the removal of RB19 in the presence of Cl^-.

$$SO_4^{\cdot-} + Cl^- \rightarrow Cl^{\cdot} + SO_4^{2-} \quad (10)$$

$$OH^{\cdot} + Cl^- \rightarrow HOCl^{\cdot-} \quad (11)$$

$$HOCl^{\cdot-} + H^+ \rightarrow Cl^{\cdot} + H_2O \quad (12)$$

$$Cl^{\cdot} + Cl^- \rightarrow Cl_2^{\cdot-} \quad (13)$$

$$HSO_5^- + Cl^- \rightarrow SO_4^{2-} + HOCl \quad (14)$$

$$HSO_5^- + 2Cl^- + H^+ \rightarrow SO_4^{2-} + Cl_2 + H_2O \quad (15)$$

Figure 10c shows the effect of added NO_3^- on the removal of RB19. At an oxidation time of 60 min, it can be seen that at a NO_3^- concentration of 1 mM, the removal of RB19 was not affected, but the removal rate decreased. However, both RB19 removal rate and RB19 removal efficiency (81.4%) decreased with increasing NO_3^- concentration to 5 mM. This decrease was attributed to the reaction of $SO_4^{\cdot-}$ and $OH^{\cdot-}$ radicals with NO_3^- to form nitrate radicals with low oxidation potential (Eqs. (16) and (17)) [61, 62].

$$NO_3^- + SO_4^{\cdot-} \rightarrow SO_4^{2-} + NO_3^{\cdot} \quad (16)$$

$$NO_3^- + OH^{\cdot} \rightarrow OH^- + NO_3^{\cdot} \quad (17)$$

Table 2 Kinetic parameters calculated in MPPBC/PMS system

Experimental conditions				First-order		Second-order		BMG		
pH	MPPBC (g/L)	PMS (mM)	RB19 (mg/L)	k_1 (min^{-1})	R^2	k_2 (L/mg/min)	R^2	1/*b*	1/*m* (min^{-1})	R^2
3	0.20	0.50	25	0.0952	0.8762	0.0079	0.9872	0.93	0.2476	0.9989
5	0.20	0.50	25	0.0088	0.7575	0.0005	0.8051	0.46	0.0663	0.9822
7	0.20	0.50	25	0.0070	0.8027	0.0004	0.8292	0.39	0.0433	0.9364
9	0.20	0.50	25	0.0047	0.8344	0.0002	0.8552	0.31	0.0195	0.9476
3	0.05	0.50	25	0.0288	0.9783	0.0021	0.9898	1.00	0.0516	0.9898
3	0.10	0.50	25	0.0390	0.9645	0.0031	0.9930	1.00	0.0759	0.9930
3	0.20	0.50	25	0.0952	0.8762	0.0079	0.9872	0.93	0.2476	0.9989
3	0.40	0.50	25	0.1228	0.8014	0.0109	0.9593	0.89	0.4035	0.9979
3	0.20	0.10	25	0.0582	0.9569	0.0046	0.9962	1.00	0.1169	0.9962
3	0.20	0.25	25	0.0624	0.9068	0.0053	0.9938	0.95	0.1522	0.9982
3	0.20	0.50	25	0.0952	0.8762	0.0079	0.9872	0.93	0.2476	0.9989
3	0.20	1.00	25	0.0736	0.9401	0.0057	0.9934	1.00	0.1472	0.9934
3	0.20	0.50	25	0.0952	0.8762	0.0079	0.9872	0.93	0.2476	0.9989
3	0.20	0.50	50	0.0484	0.9545	0.0019	0.9978	1.00	0.0956	0.9978
3	0.20	0.50	75	0.0295	0.9847	0.0007	0.9932	1.00	0.0523	0.9932

Figure 10d shows the removal of RB19 in the presence of $H_2PO_4^-$ ions. $H_2PO_4^-$ ions are the ions that affect RB19 removal the most. At 60 min oxidation time, 43.1% RB19 removal was obtained at $H_2PO_4^-$ concentration of 1 mg/L, while RB19 removal decreased to 8.3% with increasing $H_2PO_4^-$ concentration to 5 mg/L. This can be attributed to the reaction of $H_2PO_4^-$ ion with $SO_4^{\cdot-}$ and OH· radicals to form $H_2PO_4^-$ with weak redox potential (Eqs. (18) and (19)). Furthermore, $H_2PO_4^-$ ion may occupy the active sites of MPPBC, which may reduce PMS activation [51].

3.8 Kinetic Study

Kinetic studies of initial solution pH, PMS concentration, catalyst (MPPBC) dosage, and initial RB19 concentration were performed after the optimization studies were completed. First-order (Eq. (2)), second-order (Eq. (3)), and Behnajady-Modirshahla-Ghanbery (BMG) (Eq. (4)) kinetic equations were used to model the removal kinetics of RB19 in the MPPBC/PMS system. The kinetic constants were calculated using the non-linear method with the help of the Microsoft Excel Solver Add-In; the results are listed in Table 2. When the coefficients of determination (R^2) are compared, it is seen that BMG > second-order > first-order. According to these results, the BMG kinetic model is much more consistent with the experimental data to describe the removal of RB19. However, the second-order kinetic model and the BMG model have the same coefficients of determination depending on the experimental parameters. The BMG model was also applied to describe the kinetics of norfloxacin removal by PMS activation process [63].

4 Conclusions

In this study, waste recycling was achieved by converting pea pod waste into biochar and loading it with iron oxide for use as a PMS activator. Based on SEM, XRD, FTIR, and VSM analyses, the prepared MPPBC was found to contain iron oxide nanoparticles with spherical morphology, superparamagnetic properties and porous structure. In addition, the biochar loaded with iron oxide acquired magnetic properties and was very easy to separate from the solution. This increased the reusability of MPPBC. Decreasing the initial pH of the solution and increasing the catalyst dosage promoted the catalytic reaction and increased the removal rates of RB19. At an initial solution pH of 3, an MPPBC dosage of 0.20 g/L, a PMS concentration of 0.50 mM, an initial RB19 concentration of 25 mg/L, and an oxidation time of 60 min, 85% removal of RB19 was achieved. This study not only develops a recyclable and reusable biochar for the treatment of RB19 contaminated water, but also demonstrates a sustainable way to utilize agricultural waste. Future studies could investigate the effects of various metal dopants on the performance of MPPBC. Specifically, the impact of incorporating transition metals such as cobalt, nickel, and copper, in addition to iron oxide, on the catalytic activity and magnetic properties of biochar could be examined. Moreover, the effectiveness of MPPBC in PMS activation, as well as its performance in the treatment of different water pollutants and the stability of the system, could be assessed with varying metal concentrations. Such research would contribute significantly to the development of optimized and sustainable catalyst systems for the treatment of pollutants.

Acknowledgements This research has been supported by Kastamonu University Scientific Research Projects Coordination Department (Project No: KÜ-BAP01/2021-39).

Data availability Data sets generated during the current study are available from the corresponding author on reasonable request.

Declarations

Conflict of interest The author(s) declared no potential conflicts of interest with respect to the research, authorship, and/or publication of this article.

References

1. S. Wu, J. Liu, J. Li, W. You, K. Zhong, L. Feng, S. Han, X. Zhang, T. Pan, W. Liu, H. Zheng, Environ. Res. **240**, 117220 (2024)
2. J. Liu, X. Zhang, J. Li, Y. Feng, L. Feng, S. Han, T. Pan, T. Zhang, S. Wu, Z. Ke, B. Liu, H. Zheng, Environ. Res. **232**, 116271 (2023)
3. A.S. Abdulhameed, A. Hapiz, S.A. Musa, E. Kashi, R. Wu, Z.A. ALOthman, A.H. Jawad, S. Algburi, Int. J. Biol. Macromol. **256**, 128463 (2024)
4. A.H. Jawad, A.S. Abdulhameed, S.N. Surip, Z.A. Alothman, J. Cleaner Prod. **393**, 136334 (2023)
5. G.D. Değermenci, N. Değermenci, N. Emin, E. Aşıkuzun, EQA - Int. J. Environ. Qual. **47**, 40 (2022)
6. V.S. Kore, S.D. Manjare, S.V. Taralkar, J. Water Process Eng. **56**, 104472 (2023)
7. G.D. Değermenci, N. Değermenci, V. Ayvaoğlu, E. Durmaz, D. Çakır, E. Akan, J. Cleaner Prod. **225**, 1220 (2019)
8. N.A. Fathy, S.E. El-Shafey, O.I. El-Shafey, W.S. Mohamed, J. Environ. Chem. Eng. **1**, 858 (2013)
9. G.S. dos Reis, J. Thivet, E. Laisné, V. Srivastava, A. Grimm, E.C. Lima, D. Bergna, T. Hu, M. Naushad, U. Lassi, Chem. Eng. Sci. **281**, 119129 (2023)
10. Y. Liu, R. Qu, X. Li, Y. Wei, L. Feng, J. Colloid Interface Sci. **579**, 412 (2020)
11. K. Çobanoğlu, N. Değermenci, Environ. Monit. Assess. **194**, 1 (2022)
12. S. Zuo, D. Xia, Z. Guan, F. Yang, J. Zan, H. Xu, M. Huang, D. Li, Colloids Surf A Physicochem Eng Asp **611**, 125895 (2021)
13. K. Fang, L. Shi, L. Yao, L. Cui, Mater. Res. Bull. **129**, 110888 (2020)
14. M. Imran, B. Natasha, S. Murtaza, N.S. Ansar, Z.U.H. Shah, S. Khan, G. Ali, F. Boczkaj, S. Hafeez, M. Rizwan Ali, Environ. Pollut. **305**, 119291 (2022)
15. B. Zhou, J.J. Wang, P. Dangal, S. Lomnicki, A.D. Roy, J.H. Park, J. Water Process Eng. **58**, 104740 (2024)
16. H. Sun, B. Zhang, N. Wang, N. Zhang, Y. Ma, L. Zang, Z. Li, R. Xue, J. Environ. Chem. Eng. **11**, 109134 (2023)
17. L. Guo, L. Zhao, Y. Tang, J. Zhou, B. Shi, J. Environ. Chem. Eng. **10**, 106979 (2022)
18. G.D. Değermenci, Bull. Chem. Soc. Ethiop. **37**, 197 (2023)
19. A.L. Bursztyn Fuentes, F. Barraqué, R.C. Mercader, A.N. Scian, M.L. Montes, Groundw. Sustain. Dev. **14**, 100585 (2021)
20. W. Kim, C.Y. Suh, S.W. Cho, K.M. Roh, H. Kwon, K. Song, I.J. Shon, Talanta **94**, 348 (2012)
21. M. Imran, Z.U. Haq Khan, J. Iqbal, N.S. Shah, S. Muzammil, S. Ali, N. Muhammad, A. Aziz, B. Murtaza, M.A. Naeem, M. Amjad, M. Shahid, A. Zakir, M. Rizwan, Environ. Pollut. **259**, 113938 (2020)
22. H. Huang, T. Guo, K. Wang, Y. Li, G. Zhang, Sci. Total. Environ. **758**, 143957 (2021)
23. R. Gurav, S.K. Bhatia, T.R. Choi, Y.L. Park, J.Y. Park, Y.H. Han, G. Vyavahare, J. Jadhav, H.S. Song, P. Yang, J.J. Yoon, A. Bhatnagar, Y.K. Choi, Y.H. Yang, Bioresour. Technol. **297**, 122472 (2020)
24. S. Liu, S. Peng, B. Zhang, B. Xue, Z. Yang, S. Wang, G. Xu, RSC Adv. **12**, 9587 (2022)
25. Y. di Chen, Y.C. Lin, S.H. Ho, Y. Zhou, N. Qi Ren, Bioresour. Technol. **259**, 104 (2018)
26. M. Aliahmad, N. Nasiri Moghaddam, Mater. Sci. Pol. **31**, 264 (2013)
27. H. Samaraweera, D. Andrena, K. Carter, T. Felder, S. Nawalage, I. Chui, F. Perez, A. Khan, T. Mlsna, Groundw. Sustain. Dev. **21**, 100945 (2023)
28. K.W. Jung, B.H. Choi, T.U. Jeong, K.H. Ahn, Bioresour. Technol. **220**, 672 (2016)
29. A. Magdy, Y.O. Fouad, M.H. Abdel-Aziz, A.H. Konsowa, J. Ind. Eng. Chem. **56**, 299 (2017)
30. Y. Wang, L. Qiao, X. Zhang, Z. Liu, T. Li, H. Wang, Sep. Purif. Technol. **328**, 125077 (2024)
31. C. Liang, H.W. Su, Ind. Eng. Chem. Res. **48**, 5558 (2009)
32. L.W. Matzek, K.E. Carter, Chemosphere **151**, 178 (2016)
33. S. Liu, C. Zhao, Z. Wang, H. Ding, H. Deng, G. Yang, J. Li, H. Zheng, Chem. Eng. J. **386**, 124015 (2020)
34. L. Xu, C. Wu, P. Liu, X. Bai, X. Du, P. Jin, L. Yang, X. Jin, X. Shi, Y. Wang, Chem. Eng. J. **387**, 124065 (2020)
35. T. Song, X. Kang, C. Guo, Z. He, M. Ge, J. Environ. Chem. Eng. **11**, 109087 (2023)
36. R. Ma, Z. Chen, W. Xu, R. Yu, Y. Zhang, F. Chen, X. Peng, B.J. Ni, J. Qian, J. Cleaner Prod. **442**, 140885 (2024)
37. L. Yang, L. Xu, X. Bai, P. Jin, J. Hazard. Mater. **365**, 107 (2019)
38. F. Cheng, P. Zhou, X. Huo, Y. Liu, Y. Liu, Y. Zhang, J. Colloid Interface Sci. **580**, 540 (2020)
39. J. Lu, Y. Zhou, Y. Zhou, Chem. Eng. J. **422**, 130126 (2021)
40. K.Y.A. Lin, M.T. Yang, J.T. Lin, Y. Du, Chemosphere **208**, 502 (2018)
41. Y. Li, S. Ma, S. Xu, H. Fu, Z. Li, K. Li, K. Sheng, J. Du, X. Lu, X. Li, S. Liu, Chem. Eng. J. **387**, 124094 (2020)
42. Q. Wang, Y. Shi, S. Lv, Y. Liang, P. Xiao, RSC Adv. **11**, 18525 (2021)
43. L. Liu, H. Mi, M. Zhang, F. Sun, R. Zhan, H. Zhao, S. He, L. Zhou, Chem. Eng. J. **407**, 127201 (2021)
44. L. Wu, Y. Yu, Q. Zhang, J. Hong, J. Wang, Y. She, Appl. Surf. Sci. **480**, 717 (2019)
45. C. Zhang, Z. Yu, X. Wang, B. Wang, J. Hazard. Mater. **445**, 130593 (2023)
46. T.B. Nguyen, T.K.T. Nguyen, C.W. Chen, W.H. Chen, X.T. Bui, S.S. Lam, C.D. Dong, Bioresour. Technol. **382**, 129182 (2023)
47. A. Kumar, B. Prasad, Sep. Purif. Technol. **279**, 119677 (2021)
48. F. Yu, Y. Guo, J. Yang, Mater. Today Commun. **37**, 107296 (2023)
49. R. Shokoohi, K. Godini, Z. Latifi, Inorg. Chem. Commun. **149**, 110400 (2023)
50. L. Hu, G. Deng, W. Lu, Y. Lu, Y. Zhang, Chinese J. Catal. **38**, 1360 (2017)
51. J. Sun, D. Zhang, D. Xia, Q. Li, Chem. Eng. J. **471**, 144832 (2023)
52. X. Luo, M. Shen, J. Liu, Y. Ma, B. Gong, H. Liu, Z. Huang, J. Cleaner Prod. **294**, 126372 (2021)
53. H. Fu, S. Ma, P. Zhao, S. Xu, S. Zhan, Chem. Eng. J. **360**, 157 (2019)

54. H. Li, S. Li, L. Jin, Z. Lu, M. Xiang, C. Wang, W. Wang, J. Zhang, C. Li, H. Xie, J. Environ. Chem. Eng. **10**, 107085 (2022)
55. J. Wang, S. Wang, Chem. Eng. J. **411**, 128392 (2021)
56. Q. Zhu, K. Zhang, J. Xu, X. Wei, L. Shi, Sumita, C. Li, E. Lichtfouse, Water Switzerland. **15**, 1849 (2023)
57. H. Fu, P. Zhao, S. Xu, G. Cheng, Z. Li, Y. Li, K. Li, S. Ma, Chem. Eng. J. **375**, 121980 (2019)
58. J. Xu, S. Hu, L. Min, S. Wang, Water Sci. Technol. **85**, 3271 (2022)
59. Y. Yang, J.J. Pignatello, J. Ma, W.A. Mitch, Environ. Sci. Technol. **48**, 2344 (2014)
60. J.E. Grebel, J.J. Pignatello, W.A. Mitch, Environ. Sci. Technol. **44**, 6822 (2010)
61. J. Luo, S. Bo, Y. Qin, Q. An, Z. Xiao, S. Zhai, Chem. Eng. J. **395**, 125063 (2020)
62. P. Neta, R.E. Huie, A.B. Ross, J. Phys. Chem. Ref. Data **17**, 1027 (1988)
63. M. Xu, J. Yang, Y. Wang, B. Lu, R. Chen, H. Liu, Sep. Purif. Technol. **300**, 121822 (2022)